Vol. 18 No. 96 *Journal of the Radio Research Laboratories* *March 1971*
Printed in Tokyo, Japan pp. 87-111

UDC 551.524.7

MEASUREMENT OF SKY NOISE TEMPERATURE AT 16 GHz AND 35 GHz*

By

Yuichi OTSU

(Received March 27, 1970)

ABSTRACT

An experiment on the 16 GHz and 35 GHz radiometers in use for the AST-V Millimeter Wave Experiment was carried out at Goddard Space Flight Center during June and July, 1969, to measure sky noise temperature and to estimate the antenna loss factor which causes apparent increase in temperature measurement.

There is described the relation between the rainfall rate at one point and rise in temperature due to rain and rain cloud.

Some aspects of temperature scintillation due to cloud are also discussed. Calculation of sky noise temperature was made on the standard atmospheric model and other precipitation conditions.

1. Introduction

New and higher frequencies in the microwave region (over 10 GHz) are neccessary for the future space-to-ground communication. At these microwave frequencies, there exist many disturbances in the atmosphere. For example, atmospheric gaseous attenuation and precipitation losses are much greater at frequencies over 30 GHz than at frequencies around 10 GHz. Therefore, it is the fundamental necessity to investigate the character of propagation through the atmosphere at these microwave frequencies. One of equipments used for such investigation is a radiometer. It shows the noise temperature of the sky at a certain frequency, which corresponds exactly to the attenuation through the atmosphere. Thus the radiometer is very useful for investigating the character of millimeter wave space communication links. The purpose of this experiment was to find the antenna and feeder losses of the 16 GHz and 35 GHz radiometers that will provide comparative data for the ATS-V Millimeter Wave Experiment, and to provide some information on temperature increase due to rain and cloud. Calculation of sky noise temperature on clear, cloudy, and rainy days was made by the use of some standard models of the atmosphere.

* This work was carried out while the author was staying at NASA Goddard Space Flight Center, Greenbelt, Maryland, U. S. A., from Nov. 1968 to Jan. 1970.

2. Description of Systems

The two radiometers in use for the NASA AST-V Millimeters Wave Experiment at Rosman, North Carolina, U. S. A., were put in operation at Goddard Space Flight Center (GSFC), Greenbelt, Maryland, for the preliminary measurement of sky noise temperature along with calibration and checking of the system stability. The diagrams and characteristics of the two radiometers are shown in Fig. 2. 1 and Table 2. 1. These radiometers are of usual "Dicke" type, and the principal difference between two radiometers is the mechanical modulator at 16 GHz and the ferrite modulator at 35 GHz, as shown in Fig. 2. 1.

Table 2. 1. Characteristics of the Two Radiometers

Characteristics	16 GHz Radiometer	35 GHz Radiometer
Antenna	TRG* Lens antenna	TRG* Lens antenna
Diameter	12 inches	12 inches
Gain	32 dB	39 dB
Matching (VSWR)	<1. 01	<1. 01
Antenna efficiency	~0. 8	~0. 8
Beam width	4. 0°	2. 0°
RF Amplifier	T. D. A. 15 dB (NF 7 dB)	Not used
IF Amplifier		
Center frequency	160 MHz	3. 0 GHz
Bandwidth	80 MHz	2. 0 GHz
Noise figure	6 dB	12 dB
Local Oscillators	Klystron (Varian*)	Klystron (Varian*)
Modulator	Mechanical rotating	Ferrite switching
Modulator frequencies	94~100 Hz	94~100 Hz
Recorder		
Amplifier	Lock-in amplifier	Lock-in amplifier
Output voltage	0~5 V	0~5 V
Sensitivity $\left(=K\frac{T_{sys}}{\sqrt{Bt}}\right)$ (t=1 sec, k=2)	0. 22°K	0. 45°K
Ambient temperature of radiometer (RF, IF)	40°C ±1°C	
Hot load	318°K (45°C)	
Cold load	Liquid nitrogen (77°K), dry ice (198°K) or ice cubes (273°K)	

* TRG and Varian are the name of a factory.

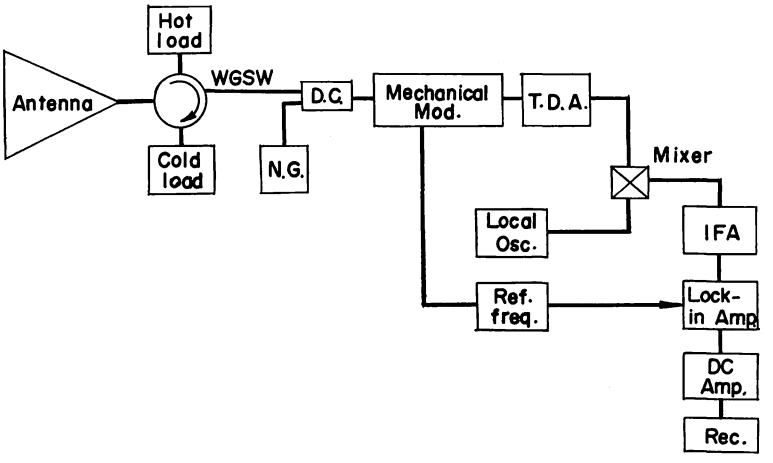

Fig. 2.1. (a). Block diagram for 16 GHz radiometer.

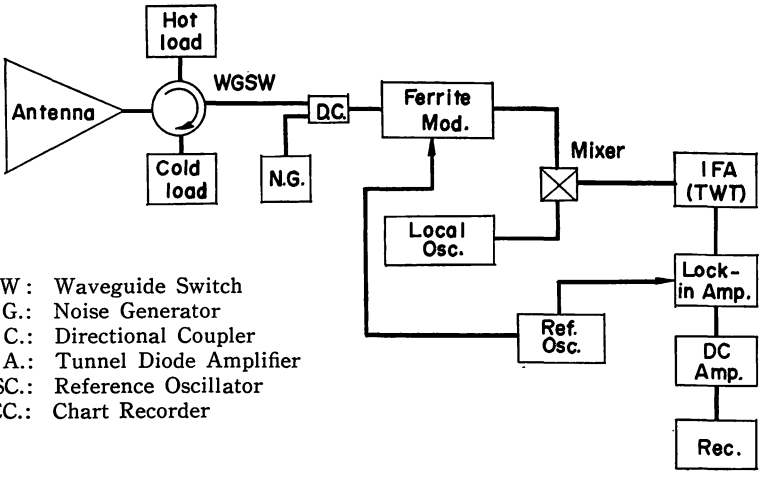

WGSW: Waveguide Switch
N. G.: Noise Generator
D. C.: Directional Coupler
T. D. A.: Tunnel Diode Amplifier
REF. OSC.: Reference Oscillator
REC.: Chart Recorder

Fig. 2.1. (b). Block diagram for 35 GHz radiometer.

In the experiment at GSFC, the radiometers were located at a parking lot adjacent to Building as shown in Fig. 2.2 in the direction of NNW, and the elevation angle was 45 degree. The location of other buildings and surrounding trees is also shown in Fig. 2.2. Measurements of ground temperature, humidity, and rainfall rate, with a tipping bucket type gauge, were made by using instruments located near the radiometers. These measurements were always checked with the Weather Bureau data in Washington, D. C.

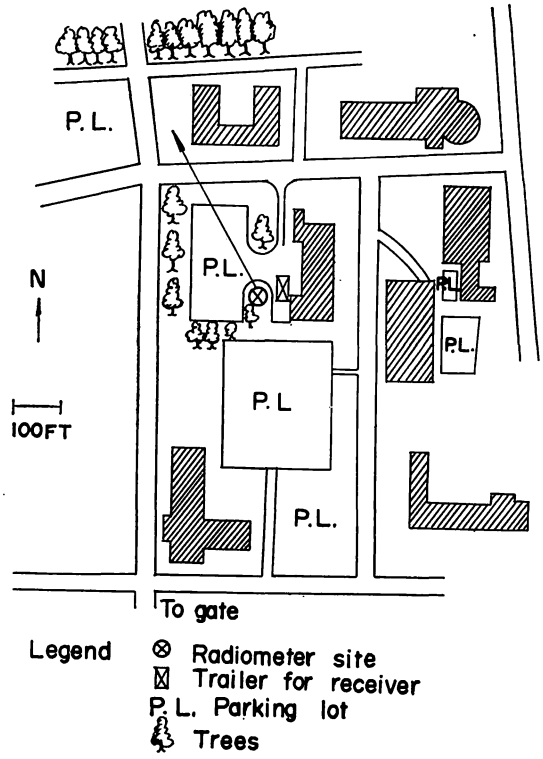

Fig. 2.2. Enlarged view of the experimental site at GSFC.

3. Correction to the Measured Sky Noise Temperature in Consideration of Wave Guide Losses

3.1. Correction to the measured sky noise temperature

For accurate measurement of the sky noise temperature, the waveguide losses must be known because they appear as a certain increase in temperature on the recorder. The waveguide losses in hot and cold load were measured by the power meter method at 16 and 35 GHz. These data are given in Tables 3.1 and 3.2.

3.1.1. Correction to the 16 GHz radiometer data

First, by the use of the values in Table 3.1, Dicke temperature on the recorder is derived from the equation (3.1) as follows:

$$T_d = T_s \cdot \alpha + T_{amb} \cdot (1-\alpha) \tag{3.1}$$

where

T_d: Dicke temperature (temperature at the input of Dicke switch or modulator),

T_s: Sky noise temperature,

T_{amb}: Ambient temperature inside the receiver box, which causes the apparent temperature increase upon Dicke temperature.

Table 3.1. 16 GHz feeder losses

Waveguide connection	Loss (dB)	Fractional transmission coefficient (α)	$1/\alpha$
Antenna to Modulator	0.9	0.813	1.23
Hot load to Modulator	0.95	0.804	1.24
Cold load to Modulator	1.15	0.767	1.30

Table 3.2. 35 GHz feeder losses

Waveguide connection	Loss (dB)	Fractional transmission coefficient (α)	$1/\alpha$
Antenna to Modulator	1.30	0.741	1.35
Hot load to Modulator	1.40	0.725	1.38
Cold load to Modulator	1.40	0.725	1.38

Dicke temperature of hot load "T_{dh}" is 317°K, which is derived from equation (3.1), putting $T_s=318$°K and $\alpha=0.804$ into the equation. In the same way, Dicke temperature of cold load "T_{dc}" is 132° K.

On the assumption that the scale of the recorder is linear (see Appendix A), the sky noise temperature, T_s, can be determind by T_d at a certain time on the recorder as follows:

$$T_s=1.23\cdot T_d-72 \tag{3.2}$$

In equation (3.1) $\alpha=0.813$, and $T_{amb}=313$° K.

Equation (3.2) must be revised later because of the assumed antenna loss.

3.1.2. Correction to the 35 GHz radiometer data

By the use of equation (3.1), Dicke temperature "T_{dh}" for the hot load and "T_{dc}" for the cold load, and "T_s" for the sky noise temperature are calculated as described in section 3.1.1.

For the hot load: $T_{dh}=317$° K,
$\alpha=0.725$, $T_{amb}=313$° K, and $T_s=318$° K,

For the cold load: $T_{dc}=142$° K,
$\alpha=0.725$, $T_{amb}=313$° K, and $T_s=77$° K,

For the antenna: $T_s=1.35\cdot T_d-110$ (3.3)

The equation (3.3) is also subject to change as mentioned in 3.1.1.

3.2. Comparison between the measured sky noise temperature and the expected sky noise temperature

After calibration with hot and cold loads, the sky noise temperature can be

obtained by equations (3. 2) and (3. 3) in section 3. 1.

In this case, antenna losses are assumed to be 0.9 dB for 16 GHz, and 1.3 dB for 35 GHz. Thus the exact loss must be measured in order that the true values of sky noise temperature may be estimated. Many ways of evaluating the antenna loss can be found, but it is the easiest way to compare the expected value with the measured one (including some assumption). The expected sky noise temperature was calculated by converting the vertical loss measured by Altshuler, et al. [2] into the sky noise temperature at 45° elevation angle, and details are described later in section 5. 2. The difference between the expected and measured values can be regarded as partly due to the antenna and waveguide losses and partly due to the antenna pattern. The differences between the measured and expected sky noise temperatures are shown in Tables 3. 3 and 3. 4. These Tables contain the date and time of measurement, absolute humidity, expected and measured sky noise temperatures, and in the Reference column, the sky noise temperature calculated by this author as described in section 5. 2.

The 16 GHz radiometer indicated large differences in temperature before and after calibration. This may have been due to the observed intermittent malfunction of the waveguide switch. The averages of differences between the measured and expected sky noise temperatures are 35° K at 16 GHz and 23° K at 35 GHz. Accordingly, equations (3. 2) and (3. 3) must be changed, these differences being taken into account. The true sky noise temperatures at 16 GHz and 35 GHz, using

Table 3. 3. Comparison between the Measured and Expected Sky Noise Temperatures for 16 GHz at 45° Elevation Angle

Date	Time	Absolute humidity (g/m^3)	Expected sky noise temperature (°K)	Measured sky noise temperature (°K) $\alpha=0.741$	Temperature difference (°K)	Reference values: Calculation by the equations of Bean and Dutton (°K)
6/25	16:50	15	11	B37	26	(8)
			11	A46	35	
6/26	16:30	16	11	45	34	(8.5)
6/28	16:30	19	12	51	39	9.5
6/29	18:30	10	9	53	44	(6.5)
6/30	17:05	11	9	B54	45	(7)
			9	A70	61*	
7/ 1	17:40	13	10	B64	54*	7.5
			10	A46	36	
7/ 2	16:20	11.5	9	B34	15	7
			9	A39	30	

* : Wave guide switch malfunction
B : Before calibration
A : After calibration
( ) : Interpolated
Average temperature difference : 35°K
(For the calculation of the average value, the data with "*" are neglected.)

Table 3.4. Comparison between the Measured and Expected Sky Noise Temperatures for 35 GHz at 45° Elevation Angle

Date	Time	Absolute humidity (g/m^3)	Expected sky noise temperature (°K)	Measured sky noise temperature (°K) $\alpha=0.813$	Temperature difference (°K)	Reference values: Calculation by the equations of Bean and Dutton (°K)
6/25	16:50	15	32	64	32	32
6/26	16:30	16	33	60	27	(33)
6/27	17:30	18	35	60	25	36
6/28	16:30	19	35	71	36*	(37)
6/29	18:30	10	26	51	25	(26)
6/30	17:05	11	27	B50	23	(27)
				A77	50*	
7/ 1	17:40	13	30	48	18	(30)
7/ 2	16:20	11.5	28	40	12	28
7/ 3	16:00	12	29	B68(CL)	39*	(28)
				A50	21	

* : Wave guide switch malfunction
B : Before calibration
A : After calibration
( ) : Interpolated
CL : Partly cloudy
Average temperature difference : 23°K
(For the calculation of the average value, the data with "*" are neglected.)

the same values of Dicke temperature T_d on the recorder as in equations (3.2) and (3.3), are as follows:

$$16\,\text{GHz} \qquad T_s=1.39\cdot T_d-121 \qquad (3.2A)$$

$$35\,\text{GHz} \qquad T_s=1.50\cdot T_d-157 \qquad (3.3A)$$

As mentioned already, these differences are due to the antenna patterns and antenna and feeder losses, including those of the waveguide switches. In consideration of the antenna patterns and their energy distribution to be shown in Appendix C, increase in temperature due to the antenna patterns and circumstantial features could be estimated roughly at 4.5° K for 16 GHz radiometer and at 12° K for 35 GHz radiometer.

4. Increase in Sky Noise Temperature due to Rain and Cloud

4.1. Increase in temperature due to rain

The relations between 10-minute average temperature increase and 10-minute average rainfall rate at the receiving point are shown in Figs. 4.1 through 4.3. One of these (Fig. 4.1) seems to be in good correlation with other experimental

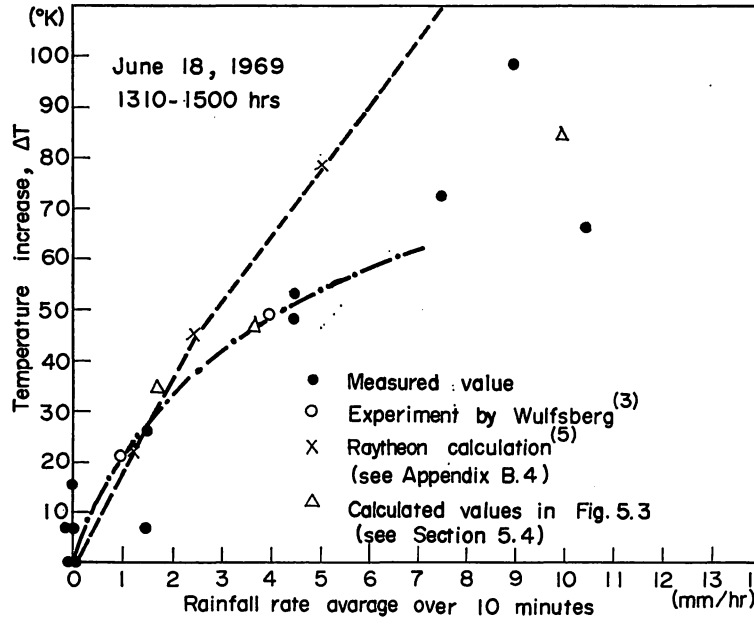

Fig. 4.1. Rainfall rate vs. temperature increase for 16 GHz.

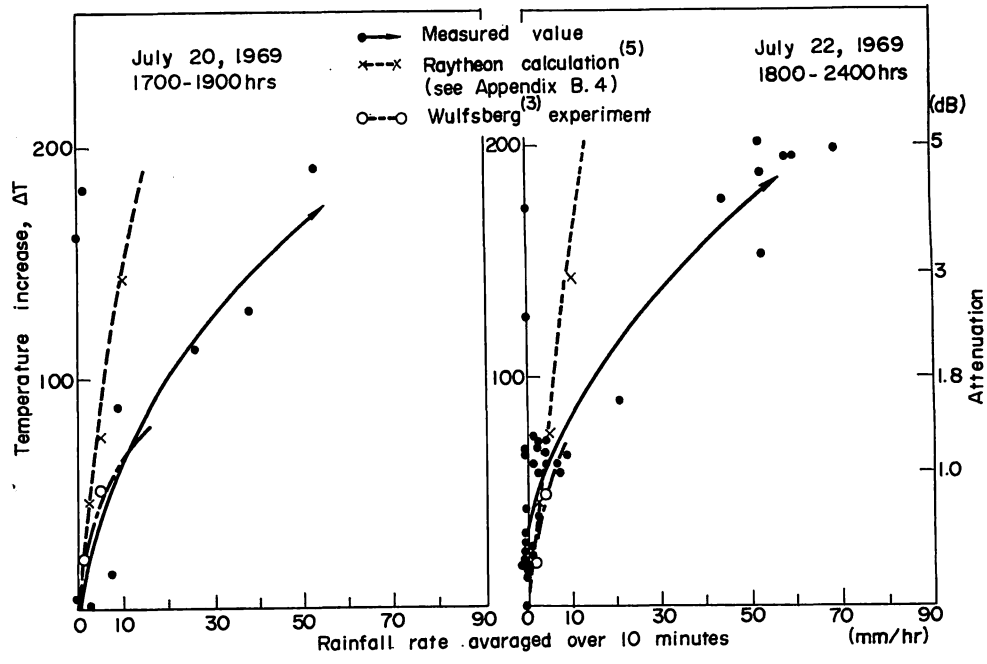

Fig. 4.2. Rainfall rate vs. temperature increase for 16 GHz.

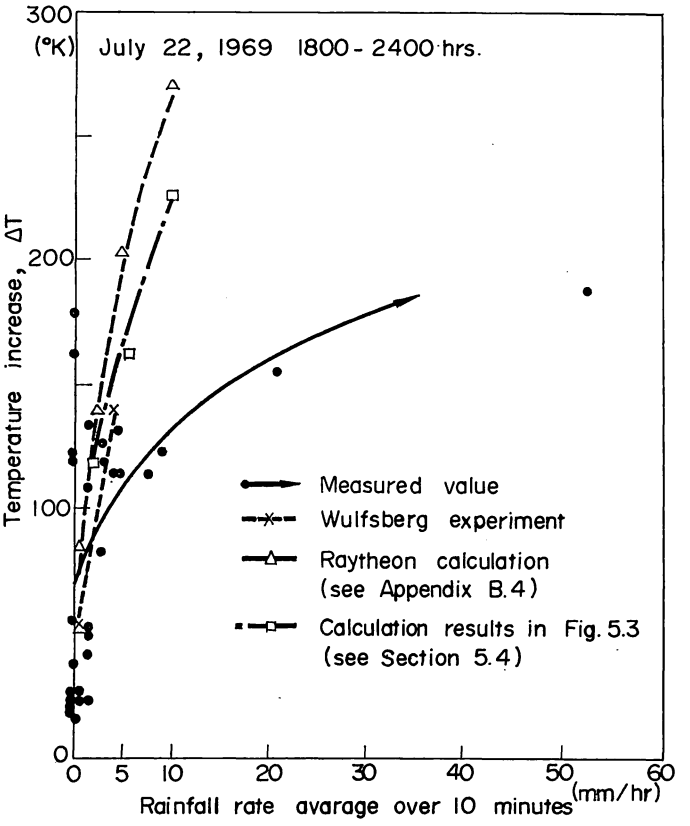

Fig. 4.3. Rainfall rate vs. temperature increase for 35 GHz.

data[3], and to be near the theoretical value[5] under 5 mm/h. But most of the rain data were much below the Raytheon theoretical values[5]. Rain starting at the site always delayed, compared with the starting time of temperature increase, when it rained heavily (see Fig. 4.4). Therefore, the correlation between rainfall rate and temperature rise was not good at that time, and the temperature rose quickly to the highest near to the ground temperature, within 4 minutes at 35 GHz and in 8 minutes at 16 GHz. (See also Fig. 4.4.)

In consideration of Figs. 4.1 through 4.3, if the rainfall rate is less than 10 mm/h, the correlation between the rainfall rate at one point and the sky noise temperature rise seems to be good even at the 45° elevation angle. This tendency is seen in other experimental data[3] and can be ascertained by the calculation of reference 5 and Fig. 5.3. This is of course due to the widespread structure of light rain. In a heavy rain, the rain cell is smaller and usually the measured temperatures at slant angles are less than calculated values, derived from one point rainfall rate on the assumption that the rainfall rate is uniform over the area considered. This is to be understood by an example of rain structure[5] as follows:

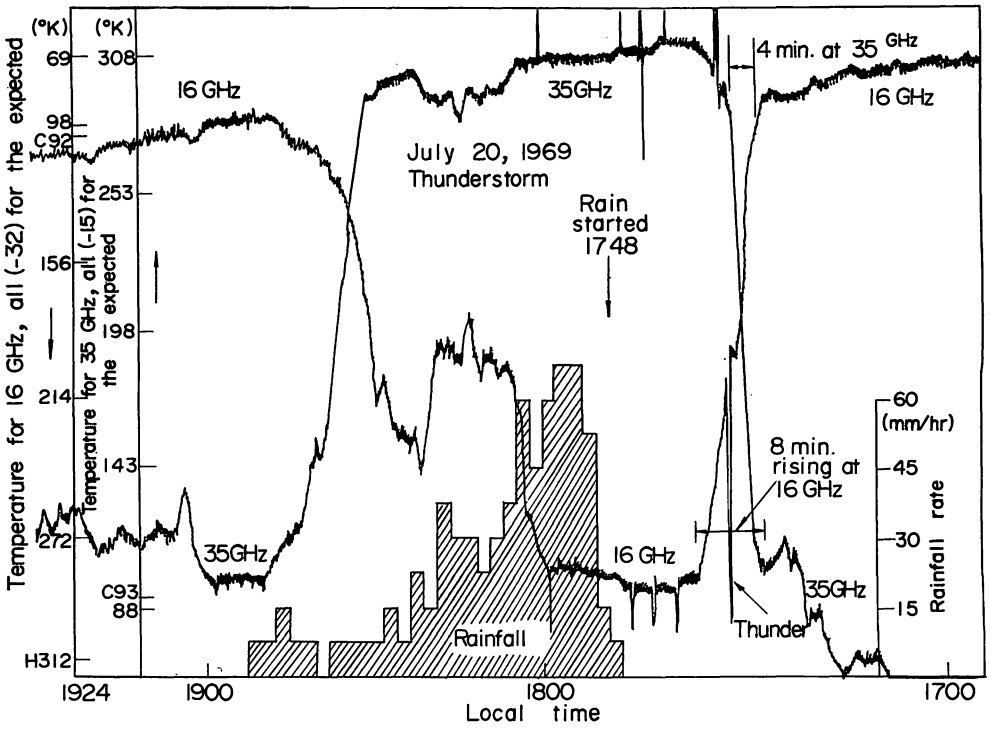

Fig. 4.4. Plot of temperature (°K) vs. time for 16 GHz and 35 GHz on July 20. (Shaded area represents rain).

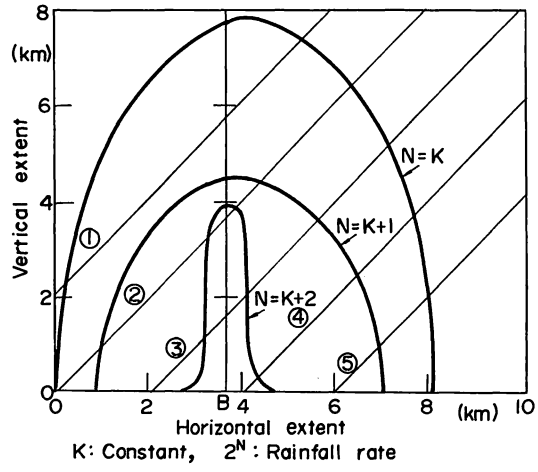

Fig. 4.5. One of Raytheon models; profile of heavy rain structure.

Raytheon model[5] for heavy rain structure as seen in Fig. 4.5 shows that the point B has the maximum rainfall rate, but the propagational loss for 45° elevation angle at the point B (path 4) becomes smaller, about 60% of the vertical loss, at 35 GHz.

But in Fig. 4.5, the slant path loss of 45° elevation becomes the largest along the line 2, about 80% of the vertical loss at the point B. Therefore, observation at a certain elevation angle shows less increase in temperature than the calculated value from the ground rainfall rate during a heavy rain of structure like in Fig. 4.5.

In consideration of one-point rainfall rate and one-point radiometer temperature increase at a certain elevation angle, it would be useful to find the cross-correlation with varying time delay between the measured temperature increase and rainfall rate, because such a heavy rain as in Fig. 4.5 moves in a certain direction with a certain speed. If the best correlation can be found for certain value of time delay, it may be possible to deduce the storm speed from the value.

4.2. Increase in temperatue due to cloud

4.2.1. Scintillation by cloud

These radiometers have an integration time of a second, but scintillation within 1 minute is mostly due to the receiver noise fluctuation, and the period of scintillation with the cloud movement is usually longer than 1 minute. A ten-minute interval was chosen for the cloud scintillation here. Further, the maximum-to-minimum temperature range within ten minutes was measured and a comparison was made between the temperature ranges at 35 GHz and at 16 GHz.

(1) Distribution of scintillation numbers

The scintillation number is defined as the number of crossing the average temperature line in each 10-minute interval on the sky noise temperature record, when clouds intersect the radiometer beam. In Table 4.1 (a) and (b) are shown the scintillation numbers per 10 minutes versus the number of occurrences. These numbers were measured at 45° elevation angle without rain during the period of experiment (from June 18 through July 31, 1969).

The scintillation numbers covering 90% of all the measurement data are 4 at 16 GHz and 5 at 35 GHz. The scintillation number 1 for 10 minutes covers almost 40% of the total measurement data for both radiometers. Therefore, we can conclude that cloud often comes into the radiometer antenna beams in large clumps.

This scintillation can be regarded as the typical effect of cloud upon the radiometers. The average scintillation numbers of all the measurement data are 2 for 10 minutes at 16 GHz and 3 for 10 minutes at 35 GHz.

The averaged temperature increase with cloud are 6° K at 16 GHz and 14° K at 35 GHz. At 35 GHz, the average temperature increase, 14° K, is in the middle of the range of data, 5° K — 25° K, measured by K. N. Wulfsberg, A. F. C. R. L.[3]

(2) Temperature distribution in the scintillation number 1

The temperature distribution in the scintillation number 1 (Table 4.2 (a) and (b)) shows that increase less than 10° K covers 92% of all the temperature increases due to cloud at 16 GHz, and that increase less than 30° K occupies 90% of

all increases at 35 GHz.

The remaining 10% are caused by rain cloud (Nimbostratus).

Table 4.1. Scintillation Number Distribution within 10 Minutes

(a) For 16 GHz

Number	Occurrence	Percent	Average Temperature Increase
1	49	36.0	6.6°K
2	39	28.6	4.3
3	24	17.6	9.5
4	13	9.6	5.0
5	3	2.2	6.0
6	7	5.1	4.7
7	0	0	0
8	1	0.7	3.0
Weighted Average of Scintillation Number	2.2	(100%)	6.1°K

(Average increase)

(b) For 35 GHz

Number	Occurrence	Percent	Average Temperature Increase
1	82	42.2	15.6°K
2	16	8.2	11.9
3	29	14.9	13.4
4	28	14.5	12.1
5	17	8.8	17.0
6	6	3.1	13.0
7	9	4.6	11.5
8	2	1.0	18.5
9	1	0.5	13.0
10	4	2.0	16.3
Weighted Average of Scintillation Number	2.9	(100%)	14.3°K

(Average increase)

Table 4.2. Distribution of Scintilation Number 1 for 10 Minutes

(a) 16 GHz

Increment	Number of Occurrences	%
40 → 50°(K)	0	
30 → 40	1	
20 → 30	2	
10 → 20	1	
0 → 10	45	92

(b) 35 GHz

Increment	Number of Occurrences	%	
100 →110°(K)	1		
90 →100	0		
80 → 90	1		
70 → 80	1		
60 → 70	2		
50 → 60	2		
40 → 50	0		
30 → 40	1		
20 → 30	9	11	≈90%
10 → 20	21	26	
0 → 10	42	52	

4.2.2. Temperature increase due to big clumps of clouds and its duration

The temperature increase "ΔT" due to big clumps of clouds and its duration are defined in Fig. 4.6. In Table 4.3 are shown examples of temperature increase ΔT and its duration Δt for a couple of days in our experiment. These data include the temperature increase 80° K at 35 GHz, which seems to have arisen owing to the existence of some rain drops in the cloud. But most of increase in temperature are mainly caused by cumulus (i.e., local convection cloud), and the longest du-

Fig. 4.6. Changes of temperature (ΔT) due to cumulus.

Table 4.3. Examples of Temperature Increase Due to Big Clumps of Clouds and its Duration

Date	35 GHz		16 GHz		Ratio
	Δt	ΔT(°K)	Δt	ΔT(°K)	ΔT 35/ΔT 16
6/13	5.5	19	2	5	3.8
	23	82	16	24	2.9
	7	37	6	10	3.7
	2.5	16	1.5	3	5.3
	4	25	9	19	1.3
	1	10	2	3	3.3
	10	54			
6/18	3	17	4	4	4.3
	1.5	7	2	3	2.3
	3	20	4	7	2.8
6/19	2	7			
	3	7			
	16	46	17	17	2.7
	8.5	13	7	3	4.3
	11	17	7	8	2.1
					Average Ratio 3.2

ration is 20 to 30 minutes. Periods longer than this occur in case that widely spread rain cloud (Nimbostratus and other clouds) intersects the main beam of the antenna. Analysis in the case of longer periods is not made here.

The average ratio "3.2" in Table 4.3 is nearly equal to the ratio "3.9" of the calculated sky noise temperature increase due to water content in cloud at 35 GHz to the temperature increase at 16 GHz, as shown in Fig. 5.2.

5. Calculation of Sky Noise Temperature from 10 GHz to 40 GHz under Various Weather Conditions

5.1. Purpose and procedure in calculation

The expected sky noise temperatures at 16 GHz and 35 GHz in Tables 3.3 and 3.4 were obtained by Altshuler, et al.[2] through their experiment. Therefore, it is necessary to compare those values with purely theoretical values.

On microwave frequencies, for example, from 10 GHz to 40 GHz, which are intended for future communication systems, it is very useful to find the range of sky noise temperature change due to change in ground temperature and humidity for a long-term experiment.

Besides, the calculation of attenuation due to rain and cloud on the frequencies mentioned above was done for reference to the measured values. Calculation of sky noise temperature through the clear atmosphere was done by the use of equa-

tions derived by Bean and Dutton.[1] Attenuation due to water vapor and oxygen was integrated along the vertical path through the atmosphere on the standard atmospheric model[2] (see Appendix B-1). The equations by Bean and Dutton[1] and other atmospheric models with precipitation found in reference (2) and reference (5-Raytheon model) are also shown in Appendices B. 2 through B. 4.

5. 2. Results of calculation on clear days

First, the expected sky noise temperatures in Tables 3. 3 and 3. 4 were derived by changing the loss values in dB obtained by the equations (5. 1) and (5. 2) (see equations (6) and (7) in reference 2) into the sky noise temperature as follows:

$$\text{at } 15\,\text{GHz} \ \ldots\ldots\ a_1(\text{dB}) = 0.055 + 0.004 \cdot \rho \qquad (5.1)$$

$$\text{at } 35\,\text{GHz} \ \ldots\ldots\ a_2(\text{dB}) = 0.17 + 0.013 \cdot \rho \qquad (5\cdot2)$$

where ρ is water vapor content on the ground.

Change the dB value of losses, a_1 and a_2, into linear values, and the expected sky noise temperatures are obtained from the equation (5. 3) found in the paper by Wulfsberg[3].

$$T_s = (1-\alpha^{\sec\phi}) \cdot T_m, \qquad (5.3)$$

where
- T_s: sky noise temperature,
- T_m: mean noise temperature, $=1.12T_g - 50$ (T_g: ground temperature in ° K) (see references (2) and (3)),
- α: linear values of a_1 and a_2
- ϕ: zenith angle, in this case, 45 degrees.

As shown in Tables 3. 3 and 3. 4, the expected sky noise temperatures coincide well with the theoretical values derived from the equations by Bean and Dutton[1].

In Fig. 5. 1 is shown variation in sky noise temperatures due to the change of ground water vapor content (absolute humidity), and due to change in the ground

Table 5. 1. Measurement List from T. N. Report (Reference 6)

Wavelength (cm)	Vertical Att. (dB)	Experimenters
2	0. 06 — 0. 1	Wulfsberg (Radio Scidnce, Vol. 2, p. 319, 1967)
0. 87	0. 363	Aarons, Barron (IRE, Vol. 46, p. 325, 1958)
0. 86	0. 22 — 0. 32	Wulfsberg (Radio Sci., Vol. 2, p. 319, 1967)
0. 86	0. 13 — 0. 34	Kalagham and Albertini (AFCRL, 1965)
0. 86	0. 2	Copeland and Tylor (Astrophy, J., Vol. 139, p. 407, 1964)
0. 86	0. 18 — 0. 39	Gibson (IRE, Vol. 46, p. 280, 1958)
0. 86	0. 2 — 0. 6	Gibson (Astrophy. J., Vol. 137, p. 611, 1963)
0. 85	0. 15 — 0. 18	Lymn, Meeks (Astron. J., 69, p. 65-67, 1964)

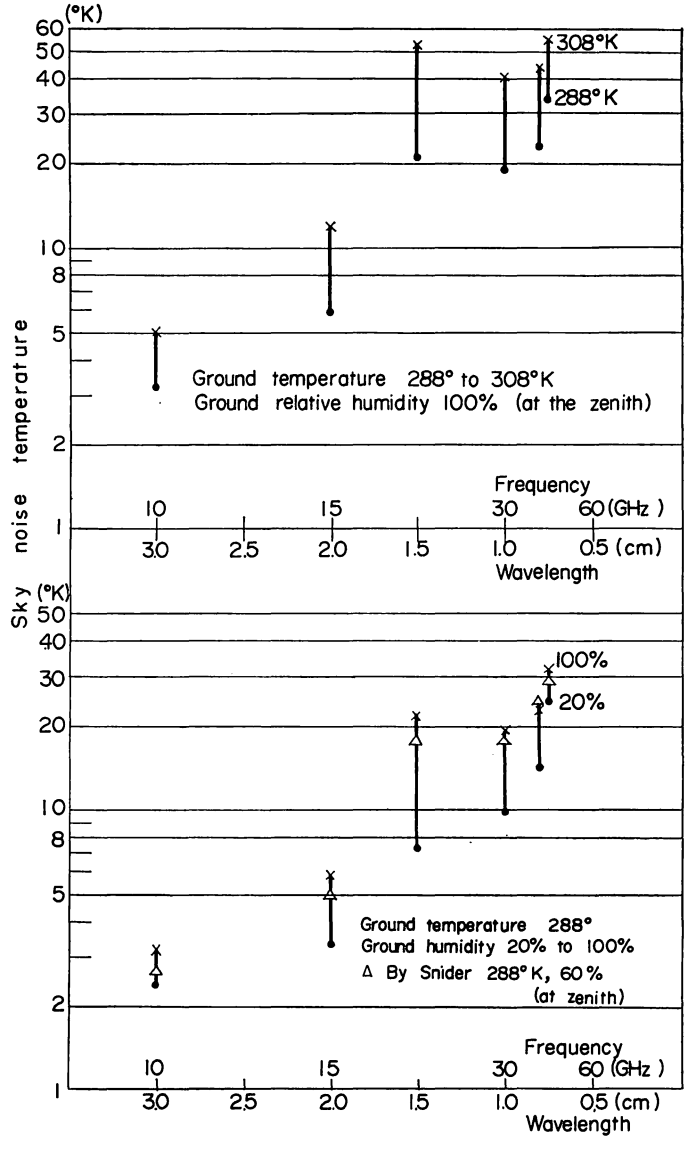

Fig. 5.1. Sky noise temperature change due to temperature and relative humidity on the ground.

temperature. For the constant ground temperature $T_g=288°$ K, sky noise temperatures vary from 3° K to 6° K at 15 GHz*, and 14° K to 23° K at 35 GHz as the relative humidity changes from 20% to 100%. And under the constant relative humidity, 100%, sky noise temperatures change from 6° K to 12° K at 15 GHz* and 23° K to 44° K at 35 GHz as the ground temperature changes from 288° K to 308° K.

* This refers to 16 GHz, and calculation was done at 15 GHz; almost no difference exists.

The total attenuation through the atmosphere, corresponding to the above-cited ranges of temperature and humidity variation, is found to be 0.05 dB to 0.18 dB at 15 GHz and 0.24 dB to 0.69 dB at 35 GHz. In Table 5.1 is shown the list of atmospheric loss measurement cited from NASA Technical Report[6]. The values of 35 GHz loss through the atmosphere are distributed from 0.13 dB to 0.6 dB. This may be explained by differences in the ground temperature and humidity each measurement.

5.3. Temperature increase due to cloud

Appendix B.3 shows a model of the atmosphere with precipitation found in the paper by Altshuler, et al.[2] This model was used for calculation of the temperature increase due to cloud on the assumption that it is not rainy, but cloud still persists. Attenuation constant for four frequencies at 0° C as shown in Table 5.2 is found in the paper by Gunn and East[7]. In the calculation of temperature increase due to cloud, ice cloud attenuation was neglected, because the loss due to ice cloud is two orders of magnitude less than the loss due to water cloud.

Fig. 5.2 shows the temperature increase due to cloud, derived by calculating all the losses along the vertical path as before. The temperature increase due to increase in water content is very prominent on the microwave frequencies as shown in this Figure.

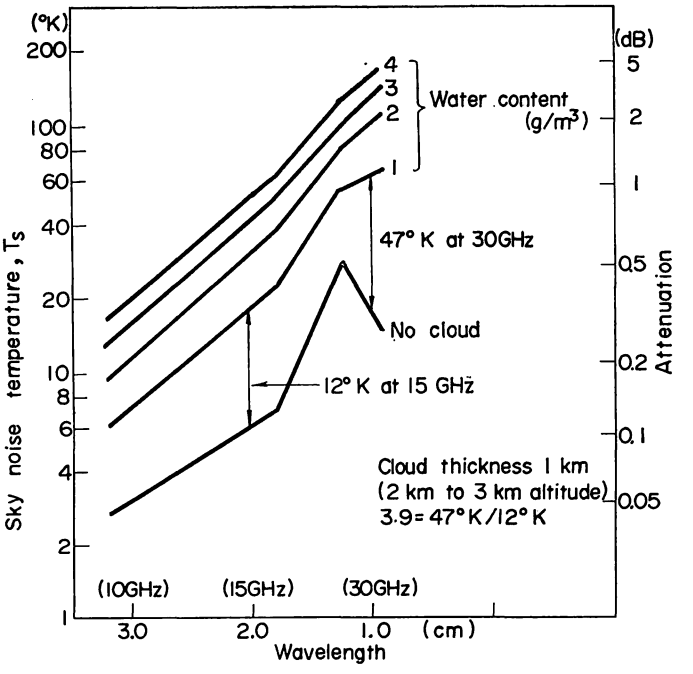

Fig. 5.2. Temperature increase due to water content in cloud. (Vertical)

Table 5.2. Attenuation due to Precipitation and Cloud
(after Gunn and East[7])

Condition of Atmosphere	Wavelength λ (cm)	3.2	1.8	1.24	0.9
Rain	Attenuation dB/km (R: mm/h)	$0.0074R^{1.31}$	$0.045R^{1.14}$	$0.12R^{1.05}$	$0.22R^{1.00}$
Water (0°C)	dB/km	$8.58\times10^{-2}M$	$26.7\times10^{-2}M$	$53.2\times10^{-2}M$	$99\times10^{-2}M$
Cloud (10°C)	M: water content (g/m³)	$6.3\times10^{-2}M$	$17.9\times10^{-2}M$	$40.6\times10^{-2}M$	$68.1\times10^{-2}M$
Ice (−10°C)	dB/km	$8.19\times10^{-4}M$	$14.6\times10^{-4}M$	$21.1\times10^{-4}M$	$29.3\times10^{-4}M$
Cloud (−20°C)	M: (g/m³)	$5.63\times10^{-4}M$	$10\times10^{-4}M$	$14.5\times10^{-4}M$	$20.0\times10^{-4}M$

Usually, however, cumulus on a fine day contains water with the average content[8] of 0.3 to 0.5 g/m³. Taking the water content of cumulus to be 0.4 g/m³ and the thickness to be 1.0 km[9], the sky noise temperature increases at 15 GHz and 35 GHz for 45° elevation angle become 3.8° K and 27° K respectively by changing the vertical temperature increase due to cloud (water content 1 g/m³) both at 15 GHz and 35 GHz as shown in Fig. 5.2, into the values in the case of water content 0.4 g/m³ at a 45° elevation angle, proportionally.

The calculated value at 16 GHz is nearly equal to the average measured temperature increase due to cloud shown in Table 4.1. But, as for the temperature increase at 35 GHz, the calculated value is about twice the average temperature increase in Table 4.1. For that reason, the equivalent thickness of cumulus at 35 GHz seems to be 0.5 km in the experiment.

5.4. Temperature increase due to rain

In case of rain are also adopted the vertical structure of cloud and rain in Appendix B.3 and attenuation constants in Table 5.2. The ground temperature and relative humidity at this time are assumed to be 293° K and 100% respectively.

The total attenuation "β" is calculated as follows:

$$\beta \text{ (in dB)} = \beta_{at} + \beta_{cl} + \beta_r \tag{5.4}$$

where
β_{at}: atmospheric gaseous attenuation,
β_{cl}: attenuation due to cloud water,
β_r: attenuation due to rain.

Calculation was done in the cases of rainfall rate from 2 mm/h to 10 mm/h, along with the constant cloud water content 1 g/m³. The results are shown in Fig. 5.3. The sky noise temperatures change from 25° to 60° K at 16 GHz and from 90° to 165° K at 33 GHz*.

* Calculation was done at 33 GHz. There was no remarkable difference between the values at 33 GHz and 35 GHz.

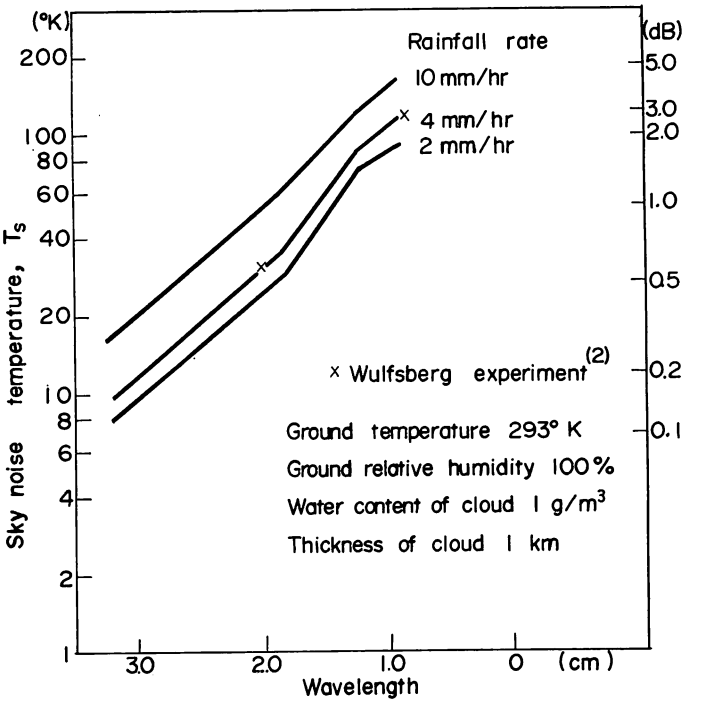

Fig. 5.3. Temperature increase due to rain.
(Vertical)

The results of calculation at 16 GHz and 35 GHz in the angle of 45° elevation are plotted in Figs. 4.1 and 4.3. The plotted values in Fig. 4.1 are in very good coincidence with the measured values. This shows that the rain at that time was stratified and wide-spread, because calculation was done by the use of the stratified model in Appendix B.3. However, the calculated values in Fig. 4.3 are far from the measured values, which shows that the rain was a kind of showers, having the structure like in Fig. 4.5 as mentioned in Section 4.1.

6. Conclusion

The average differences between the expected and measured sky noise temperatures were 35° K for the 16 GHz radiometer and 23° K for the 35 GHz radiometer. The differences include the antenna feeder loss and the temperature increase due to the side lobes of the radiometer antenna hitting the surrounding trees.

The surrounding environment being taken into consideration, the sky noise temperature increase due to the side lobes was estimated, and values of 4.5° K at 16 GHz and 12° K at 35 GHz were obtained for side lobe effects at the usual observational angle, 45 degrees from the zenith.

The correlation between one-point rainfall rate near the radiometers and the measured temperature increase due to rain at 45° elevation angle was not good dur-

ing severe thunderstorms in summer, but was much better in rather light rain (less than 10 mm/h).

Statistics on cloud scintillation per ten-minutes show that scintillation number 1 occurred most frequently. The scintillation number reached 10 at the maximum within 10 minutes.

Computation for the expected sky noise temperature shows that, under various ground conditions, change in the sky noise temperature is very small, 3° to 6° K at 15 GHz, but larger change in temperature, 14° to 23° K, appears at 35 GHz, by the equations of Bean and Dutton[1].

As for temperature increase due to rain or cloud, the water content of cloud has an important effect upon the radiometer temperature in the frequency region above 30 GHz.

Acknowledgements

This work was done during the author's stay at GSFC for about a year (Nov. 1968~Jan. 1970) with the support of all the members of the Extra High Frequency Technology Section. I tender my grateful acknowledgement to Mr. William O. Binkley, the Section Head, for his gift of opportunity of performing the radiometer experiment as an exchange visitor, and to Mr. J. Larry King who engineered the radiometers and always aided the experiment with his valuable suggestions. Further, I wish to express my heartfelt thanks to Mr. E. Hirschmann who always helped me in the experiment and took time off his busy activities for discussion on this paper, and to Dr. E. Mondre who kindly gave me many suggestions, especially for the computation of sky noise temperatures.

Last but not least, I am much obliged to Mr. James L. Baker, Ground Support Manager, ATS Project Office, for his great assistance in the negotiation for my visit to NASA GSFC.

References

(1) Bean, B. R. and Dutton, E. J., Radio Meteorology, National Bureau of Standards Monograph 92, March 1966.

(2) Altshuler, E. E., Falcone, Jr. V. J. and Wulfsberg, K. N., Atmospheric Effects on the Propagation at Millimeter Wavelengths, I. E. E. E. Spectrum, 5, pp. 83-90, July 1968.

(3) Wulfsberg, K. N., Apparent Sky Temperature Measurements at Millimeter Wave Frequencies, Physical Science Research Papers No. 38, Air Force Cambridge Research Laboratories, July 1964.

(4) Snider, J. B., Proposed Program for the Study of Atmospheric Attenuation of Satellite Signals, Environmental Science Service Administration Technical Report RL 62-WPL 1, Jan. 1968.

(5) Raytheon Company, Final Report for Millimeter Communication Propagation Program, Extension, 28 May 1966 — 27 Feb. 1967, Vol. 1, Section 1 through 3, NASA Contract No. NAS 5-9525.

(6) Thompson III, W. I., and Haroules, G. G., A Review of Radiometric Measurements of Atmospheric Attenuation at Wavelength 75 cm to 2 mm, NASA TN D-5087, Electronics Research Center, Cambridge, Mass., April 1969.

(7) Gunn, R. L. S., and East, T. W. R., The Microwave Properties of Precipitation Particles, Quat. J. Roy. Met. Soc., **80**, pp. 522-545, 1954.
(8) For Example, Mason, B. J., The Physics of Clouds, Oxford, Clarendon Press, 1957.
(9) For Example, Ishimaru, Y., Cloud Pictures and their Illustrations, published in Feb. 1954. (in Japanese)

Appendix A. Method of Calibration and Their Problems

Two cold loads were used for the linearity check on the recorder; they were:

(a) dry ice + alcohol, −75° C (198° K),

(b) ice cube + water, 0° C (273° K),

These points are shown in Fig. A. 1. This figure indicates the reasonable linearity of both radiometers.

Calibration of both radiometers was accomplished by the use of waveguide switches (WGSW). Besides difficulties in waveguide switching, some difficulties

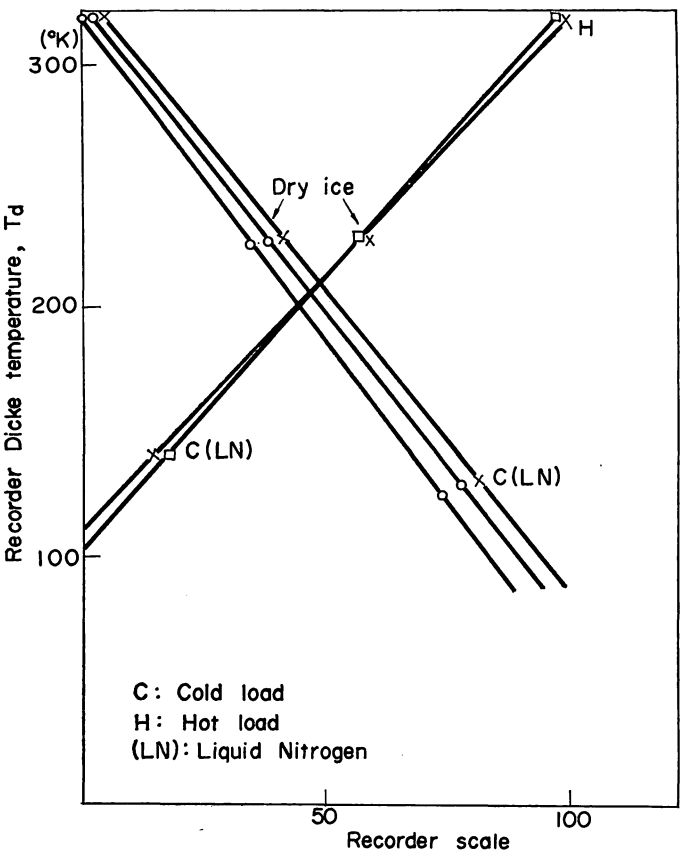

Fig. A. 1. Radiometer calibration.

of calibration in cold load occurred owing to the buildup of dewdrops inside the waveguide between the cold load and the WGSW.

During the cold load calibration, the waveguide was evacuated or filled with high-pressure helium gas to avoid the accumulation of water drops, which caused the instability of temperature.

Appendix B. 1. Standard Atmospheric Model[2]

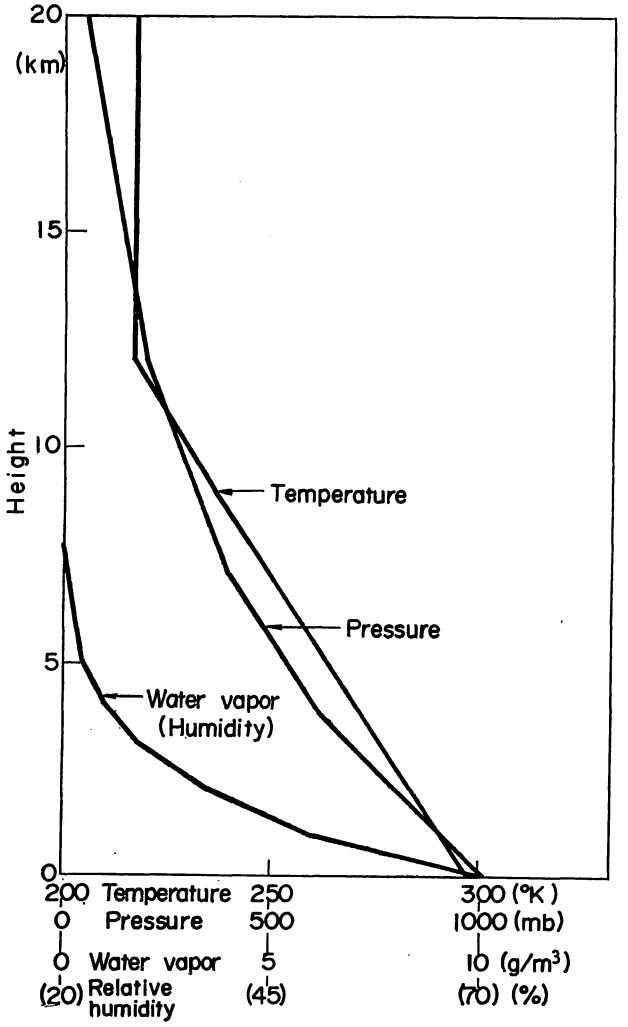

Fig. B. 1.

Appendix B. 2. Equations by Bean and Dutton

(1) Water vapor attenuation:

$$\left.\frac{\kappa}{\rho}\right|_{H_2O}=\frac{3.53\times10^{-3}}{\lambda^2}\left[\frac{\Delta\nu/c}{\left(\frac{1}{\lambda_0}-\frac{1}{\lambda}\right)^2+\left(\frac{\Delta\nu}{c}\right)^2}+\frac{\Delta\nu/c}{\left(\frac{1}{\lambda_0}+\frac{1}{\lambda}\right)+\left(\frac{\Delta\lambda}{c}\right)^2}\right]\left(\frac{293}{T}\right)^{2.5}$$

$$+\frac{0.05}{\lambda^2}\left(\frac{\Delta\nu}{c}\right)\left(\frac{293}{T}\right)$$

where κ: dB/km attenuation,
ρ: water vapor content,
λ: wave length in cm,
T: temperature at a certain height (° K),
$\Delta\nu/c=0.087\cdot(P/1013.25)\times(318/T)(1+0.0046\cdot\rho)$,
P: atmospheric pressure in millibar.

(2) Oxygen attenuation:

$$\kappa\Big|_{O_2}=\frac{0.34}{\lambda^2}\left[\frac{(\Delta\nu/c)_1}{\left(\frac{1}{\lambda_0}-\frac{1}{\lambda}\right)^2+\left(\frac{\Delta\nu}{c}\right)_1^2}+\frac{(\Delta\nu/c)_1}{\left(\frac{1}{\lambda_0}+\frac{1}{\lambda}\right)^2+\left(\frac{\Delta\nu}{c}\right)_1^2}+\frac{(\Delta\nu/c)_2}{\left(\frac{1}{\lambda}\right)^2+\left(\frac{\Delta\nu}{c}\right)_2^2}\right]\times\frac{293}{T},$$

whher κ: attenuation in dB/km
$(\Delta\nu/c)_1=0.018\times(P/1013.25)\times(293/T)^{0.75}$,
$(\Delta\nu/c)_2=0.049\times(P/1013.25)\times(293/T)^{0.75}$.

Attenuation at a certain height due to oxygen must be multiplied by ρ_{O_2} (oxygen density),

$$\rho_{O_2}=385\times0.210\times P/T.$$

Appendix B. 3. Model of the Atmosphere with Precipitation[2]

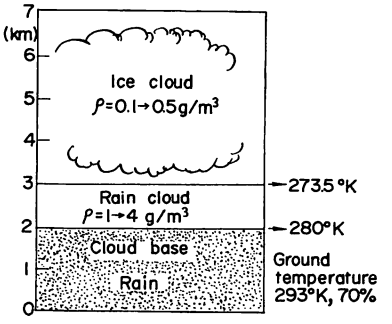

Fig. B. 3.

Appendix B. 4. Raytheon Model[5] (the altitude profile of temperature, pressure, cloud water and precipitation)

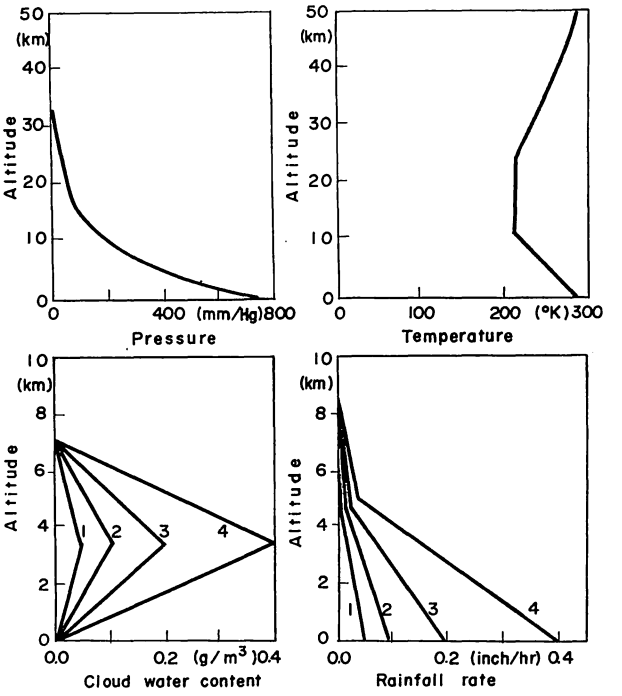

Note: Theoretical calculations were done according to this model. Two upper graphs are constant in calculation on cloudy and rainy days with various elevation angles.
Cloudy days have only the water contents in the graph on the lower left. Rainy days have both graphs at the bottom. Number 1 rain has number 1 cloud water content in the lower graphs. The rest are the same.

Fig. B. 4.

Appendix C. Energy Distribution Pattern for the Radiometer Antennas

In Fig. C. 1 are shown the antenna patterns measured in the E plane and the H plane for the 16 GHz radiometer antenna. Scale reduction into half of the 16 GHz horizontal angle values may be applied to the 35 GHz radiometer antenna (parenthetic numbers).

In the H plane pattern, the side lobes are fairly low under 30 dB, and negligible is the effective increase in temperature due to them. Therefore, only the E plane pattern needs to be consiedred for the investigation of increase in tempe-

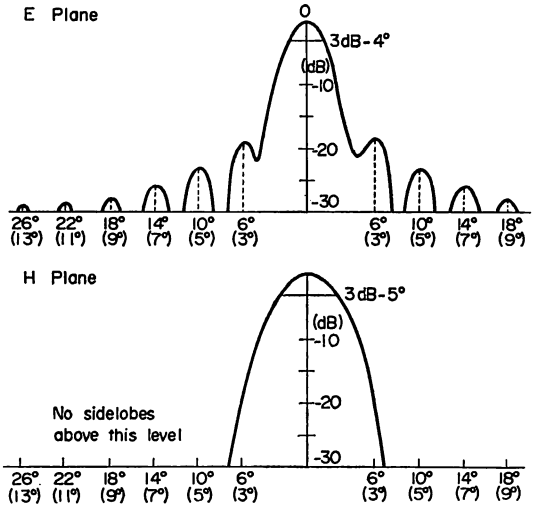

Fig. C. 1. Actual antenna pattern for 16 GHz 1-foot antenna.

Table D. 1.

Main beam	0 — + 5°	66%	For 35 GHz, angle values can be assumed to be about half of these values.
Side lobes	— + 20°	30%	
Side lobes	— + 60°	3%	
Side lobes	— +180°	1%	

rature due to side lobes. By the measurement of the area of antenna pattern, the approximate energy distribution for the 16 GHz radiometer antenna is obtained in Table D. 1.

It can be seen that 99% of all the energy falls within ±60° for the 16 GHz radiometer and within ±30° for the 35 GHz radiometer.

In the estimation of increase in temperature due to the side lobes by the use of values in Table D. 1, it is 2.5° K at 16 GHz and 7.5° K at 35 GHz at the zenith. The estimated values of side lobe effects in Section 3. 2 are for elevation angle 45°.